Shape Analysis with Multivariate Tensor-based Morphometry and Holomorphic Differentials

Yalin Wang
Dept of Neurology/Math
UCLA
ylwang@math.ucla.edu

Tony F. Chan
Dept of Math
UCLA
chan@math.ucla.edu

Arthur W. Toga
Dept of Neurology
UCLA
toga@loni.ucla.edu

Paul M. Thompson
Dept of Neurology
UCLA
thompson@loni.ucla.edu

Abstract

In this paper, we propose multivariate tensor-based surface morphometry, a new method for surface analysis, using holomorphic differentials; we also apply it to study brain anatomy. Differential forms provide a natural way to parameterize 3D surfaces, but the multivariate statistics of the resulting surface metrics have not previously been investigated. We computed new statistics from the Riemannian metric tensors that retain the full information in the deformation tensor fields. We present the canonical holomorphic one-forms with improved numerical accuracy and computational efficiency. We applied this framework to 3D MRI data to analyze hippocampal surface morphometry in Alzheimer's Disease (AD; 12 subjects), lateral ventricular surface morphometry in HIV/AIDS (11 subjects) and biomarkers in lateral ventricles in HIV/AIDS (11 subjects). Experimental results demonstrated that our method powerfully detected brain surface abnormalities. Multivariate statistics on the local tensors outperformed other TBM methods including analysis of the Jacobian determinant, the largest eigenvalue, or the pair of eigenvalues, of the surface Jacobian matrix.

1. Introduction

Three-dimensional surface-based methods have been extensively used to study face recognition [11, 24], structural features of the brain, such as cortical gray matter thickness, complexity, and patterns of brain change over time due to disease or developmental processes [16, 6]. Deformation-based morphometry (DBM) [2, 5] directly uses 2D or 3D deformations obtained from the nonlinear registration of brain images to infer local differences in brain volume or shape. Tensor-based morphometry (TBM) [7, 4] tends to examine spatial derivatives of the deformation maps registering brains to common template, constructing morphological tensor maps such as the Jacobian determinant, torsion or vorticity. DBM, by contrast, tends to analyze 3D displacement vector fields encoding relative positional differences across subjects. One advantage of TBM for surface morphometry is that surfaces are commonly parameterized using grids from which local deformation tensors can be naturally derived - TBM can even make use of the Riemannian surface metric to characterize local anatomical changes.

Using the concepts of homology and cohomology groups for general surfaces, one can convert topological problems to algebraic problems and use simple methods from linear algebra to solve them. Homology is a geometric concept and relatively easy to visualize or imagine. Cohomology is a more analytic concept, making structures easier to compute with and manipulate. In differential geometry, a holomorphic one-form (see below for detailed definitions) can be represented as a pair of scalars on each edge of a discrete mesh structure. All holomorphic one-forms form a linear space, which is isomorphic to the first cohomology group $H^1(S, \mathbb{R})$. In addition, the holomorphic one-form is an intrinsic, coordinate-free formulation. It provides a practical way to induce conformal parameterizations on surfaces and compute surface-to-surface registrations. In computational anatomy research, Wang et al. [22] used holomorphic one-forms to compute holomorphic flow segmentation, which partitions branching objects into a set of connected surface models. However, when they computed an exact harmonic one-form's conjugate one-form, a simple 90° rotation about the surface normal was used. In general, as the estimation of this surface normal was not completely accurate, this method introduced approximation errors. Holomorphic one-forms were also used to compute conformal slit maps of cortical surfaces and non-rigid human face matching and registration [21, 24].

In this paper, we present a multivariate TBM framework and apply it to detect abnormal areas on anatomical structures in the brain represented as surfaces, parameterized using differential forms (holomorphic one-forms). Our work has 3 major contributions.First, we propose a new multi-

variate TBM framework for surface morphometry, using differential forms as the basis for the tensors that are analyzed. Second, we proposed a more numerically stable and computationally efficient algorithm to compute holomorphic one-forms. And third, we performed three empirical studies of brain abnormalities in Alzheimer's Disease (AD), and HIV/AIDS. We studied hippocampal surface deformation associated with AD, and lateral ventricular surface deformation associated with HIV/AIDS. The proposed multivariate TBM detected areas of statistically significant deformation even in a relatively small test datasets - one compares 12 subjects with AD to a group of 14 matched healthy controls and the other compares 11 subjects with HIV/AIDS to 8 matched healthy controls. We also studied HIV/AIDS biomarkers based on our multivariate TBM results on lateral ventricular surfaces. With the identified biomarkers, we applied a leave-one-out test with Nearest Neighbor classifier. We achieved 100% sensitivity on both right and left surfaces and $100\%, 87.5\%$ specificity on right and left, respectively. Our goal was to show that the proposed multivariate TBM had more detection power by detecting consistent but more statistically significant areas of abnormal brain structure.

2. Theoretical Background and Definitions

Suppose S is a surface embedded in $\mathbb{R}^3$, with induced Euclidean metric $\mathbf{g}$. S is covered by an atlas $\{(U_\alpha, \phi_\alpha)\}$. Suppose (x_α, y_α) is the local parameter on the chart (U_α, ϕ_α). We say (x_α, y_α) is *isothermal*, if the metric has the representation $\mathbf{g} = e^{2\lambda(x_\alpha, y_\alpha)}(dx_\alpha^2 + dy_\alpha^2)$.

The *Laplace-Beltrami operator* is defined as

$$\Delta_{\mathbf{g}} = \frac{1}{e^{2\lambda(x_\alpha, y_\alpha)}}(\frac{\partial^2}{\partial x_\alpha^2} + \frac{\partial^2}{\partial y_\alpha^2}).$$

A function $f : S \to \mathbb{R}$ is *harmonic*, if $\Delta_{\mathbf{g}} f \equiv 0$.

Suppose ω is a real differential one-form with the representation $f_\alpha dx_\alpha + g_\alpha dy_\alpha$ in the local parameters (x_α, y_α), ω is a *closed one-form*, if on each chart (x_α, y_α), $\frac{\partial f}{\partial y_\alpha} - \frac{\partial g}{\partial x_\alpha} = 0$. ω is an *exact one-form*, if it equals the gradient of some function. An exact one-form is also a closed one-form. The de Rham cohomology group $H^1(S, \mathbb{R})$ is the quotient group between closed one-forms and exact one-forms. If a closed one-form ω satisfies $\frac{\partial f}{\partial x_\alpha} + \frac{\partial g}{\partial y_\alpha} = 0$, then ω is a *harmonic one-form*. Hodge theory claims that in each cohomologous class, there exists a unique harmonic one-form. The gradient of a harmonic function is an exact harmonic one-form.

The *Hodge star operator* turns a one-form ω into its *conjugate* ${}^*\omega$, ${}^*\omega = -g_\alpha dx_\alpha + f_\alpha dy_\alpha$. If we rewrite the isothermal coordinates (x_α, y_α) in the complex format $z_\alpha = x_\alpha + iy_\alpha$, then the isothermal coordinate charts form a *conformal structure* on the surface. Holomorphic differential forms can be generalized to Riemann surfaces by using the notion of conformal structure. A *holomorphic one-form* is a complex differential form, such that on each chart, it has the form $u = f(z)dz = \omega + \sqrt{-1}{}^*\omega$, where ω is a real harmonic one-form, $f(z)$ is a holomorphic function. All holomorphic one-forms form a linear space, which is isomorphic to the first cohomology group $H^1(S, \mathbb{R})$.

A holomorphic one-form induces a special system of curves on a surface. *Horizontal/vertical trajectories* are the curves that are mapped to iso-v/iso-u lines in the parameter domain. The trajectories that connect zero points, or a zero point with the boundary, are called *critical trajectories*. The critical horizontal trajectories form a graph, called the *critical graph*, which partitions the surface into a set of non-overlapping patches that jointly cover the surface, and each patch is either a topological disk or a topological cylinder [15]. Each patch $\Omega \subset M$ can be mapped to the complex plane by the integration of the holomorphic one-form on it.

The structure of the critical graph and the parameterizations of the patches are determined by the conformal structure of the surface. If two surfaces are topologically homeomorphic to each other and have similar geometrical structures, they support consistent critical graphs and segmentations (i.e., surface partitions), and their parameterizations are consistent as well. Therefore, by matching their parameter domains, the entire surfaces can be directly matched in 3D. This generalizes prior work in medical imaging that has matched surfaces by computing a smooth bijection to a single canonical surface, such as a sphere or disk.

2.1. Illustration on the Planar Case

Suppose we have an analytic function $\phi : z \to w, z, w \in \mathbb{C}$ maps the complex z-plane to the complex w-plane. For simplicity, we simply choose ϕ as $w = z^2$; the map is visualized in Figure 1 (a) and (b). The holomorphic one-form is the complex differential $dw = 2zdz$. The red and blue curves on the z-plane are the horizontal trajectories and vertical trajectories of dw. They are mapped to the red and blue lines on the w-plane. We examine a horizontal trajectory γ; ϕ maps γ to a horizontal line, namely, along γ the imaginary part of the differential form dw is always zero. Similarly, along a vertical trajectory, the real part of dw is always zero.

The center of the z-plane is a *zero point*, which is mapped to the origin of the w-plane. At the zero point, more than one horizontal trajectories intersect and more than one vertical trajectories intersect. The horizontal critical trajectories partition the z-plane into 4 patches. Each patch is mapped by ϕ to a half plane in w-plane.

Similarly, Figure 1 (c) shows an analytic map from a 2-hole annulus, z plane, to the complex plane, w-plane. It is visualized in the same way, i.e., the horizontal and vertical trajectories in the z are represented as red and blue curves, which are mapped to the horizontal and vertical lines in w-

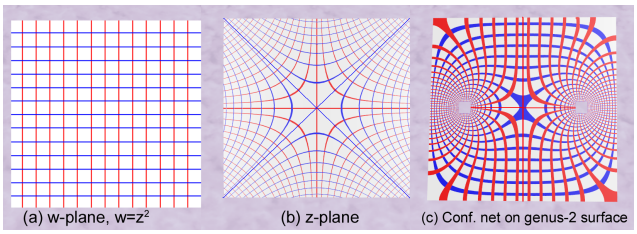

Figure 1. Trajectories on planar surfaces. (a) is the w plane. (b) illustrates trajectories of $dw = 2zdz$. (c) shows trajectories on a genus-0 surface with 3 boundaries, which is topologically equivalent to the ventricular surface after the topology change (Sec. 5.2).

plane. It is still true that the critical graph partitions the surface into a set of non-overlapping patches, each of which can be conformally mapped to the complex plane.

3. Algorithm

3.1. Holomorphic One-Forms Computation

Suppose S is an open surface with $n+1$ boundaries, $\gamma_0, \cdots, \gamma_n$. The exact harmonic one-form bases, $\{\eta_1, \eta_2, ..., \eta_n\}$, can be obtained by $\eta_k = df_k$, where $f_k : S \to \mathbb{R}$ is a harmonic function and computed by solving the Dirichlet problem on the mesh M: $\begin{cases} \Delta f_k \equiv 0 \\ f_k|_{\gamma_j} = \delta_{kj} \end{cases}$, where δ_{kj} is the Kronecker function, and Δ is the discrete Laplace-Beltrami operator using the co-tangent formula [14].

With the exact harmonic one-forms, we will compute the closed one-form basis. Fixing a boundary, γ_0, compute a path from every other boundary γ_k to γ_0, denote it by ζ_k. ζ_k cuts the mesh open to M_k, while ζ_k itself is split into two boundary segments ζ_k^+ and ζ_k^- in M_k. Define a function $g_k : M_k \to \mathbb{R}$ by solving a Dirichlet problem, $\begin{cases} \Delta g_k \equiv 0 \\ g_k|_{\zeta_k^+} = 1 \\ g_k|_{\zeta_k^-} = 0. \end{cases}$. Compute the gradient of g_k and let $\tau_k = dg_k$, then map τ_k back to M, where τ_k becomes a closed one-form. Then we need to find a function $h_k : M \to \mathbb{R}$, by solving the following linear system: $\Delta(\tau_k + dh_k) \equiv 0$. By updating τ_k to $\tau_k + dh_k$, we now have $\{\tau_1, \tau_2, \ldots, \tau_n\}$ as a basis set for all the closed but non-exact harmonic one-forms.

A simple way to compute conjugate one-forms $\{{}^*\eta_1, ..., {}^*\eta_n\}$ is to directly apply the Hodge star [22]. That is, rotating η_k by 90° about the surface normal. However, because surface normals are usually computed with numerical errors, this approximation is usually not accurate enough. From the fact that η_k is harmonic, we can conclude that its conjugate ${}^*\eta_k$ should also be harmonic. Therefore, ${}^*\eta_k$ can be represented as a linear combination of the base harmonic one-forms: ${}^*\eta_k = \sum_{i=1}^n a_i\eta_i + \sum_{i=1}^n b_i\tau_i$. Using the wedge product $\wedge$, we can construct the following linear system,

$$\int_M {}^*\eta_k \wedge \eta_i = \int_M \eta_k' \wedge \eta_i, \int_M {}^*\eta_k \wedge \tau_j = \int_M \eta_k' \wedge \tau_j.$$

We solve this linear system to obtain the coefficients a_i and b_i $(i = 1, 2, \cdots, n)$ for the conjugate one-form ${}^*\eta_k$. Pairing each base exact harmonic one-form in the basis with its conjugate, we get a basis set for the holomorphic one-form group on M: $\{\eta_1 + \sqrt{-1}{}^*\eta_1, \cdots, \eta_n + \sqrt{-1}{}^*\eta_n\}$

3.1.1 Canonical Conformal Parameterization

Given a Riemann surface M, there are infinitely many holomorphic one-forms, but each of them can be expressed as a linear combination of the basis elements. We define a canonical conformal parametrization as a linear combination of the holomorphic bases $\omega_i = \eta_i + \sqrt{-1}{}^*\eta_i$, $i = 1, ..., n$. A *canonical conformal holomorphic one-form* can be computed by

$$\omega = \sum_{i=1}^{n} \omega_i. \tag{1}$$

The conformal parametrization induced from the canonical conformal holomorphic one-form is called the *canonical conformal parametrization*. Compared with the prior work [22], the current canonical conformal parameterization directly works on open boundary surfaces and does not need to compute surface double covering and homology basis. So it is more computationally efficient.The obtained conformal parameterization maximizes the uniformity of the induced grid over the entire domain and can provides a consistent mapping across surfaces.

3.2. Two Surface Registration Methods based on Holomorphic Differentials

We can use the induced conformal parameterization for further surface analysis. There are numerous nonrigid surface registration algorithms [10] that can be applied to register each segmented surface via the parameter domain. In our work, we applied two surface registration methods: a constrained harmonic map method and a surface fluid registration method.

Given two surfaces S_1 and S_2, whose conformal parameterizations are $\tau_1 : S_1 \to R^2$ and $\tau_2 : S_2 \to R^2$, we want to compute a map, $\phi : S_1 \to S_2$. Instead of directly computing ϕ, we can easily find a harmonic map between the parameter domains. We look for a harmonic map, $\tau : R^2 \to R^2$, such that

$$\tau \circ \tau_1(S_1) = \tau_2(S_2), \tau \circ \tau_1(\partial S_1) = \tau_2(\partial S_2), \Delta\tau = 0.$$

Then the map ϕ can be obtained by $\phi = \tau_1 \circ \tau \circ \tau_2^{-1}$. Since τ is a harmonic map, and τ_1 and τ_2 are conformal maps, the

resulting ϕ is a harmonic map. For landmark curve matching, we guarantee the matching of both ends of the curves. For the other parts of these curves, we match curves based on unit speed parameterizations of both curves.

The constrained harmonic map method only considers an exact boundary mapping while using a smooth mapping in mathematically enforced regularity on inner parts. To better match surfaces via their intrinsic geometric features including conformal factor and mean curvature, we propose a surface fluid registration method [23] where surface geometric features and mutual information are used to drive a diffeomorphic fluid flow that is adjusted to find appropriate surface correspondences in the parameter domain. A diffeomorphic surface-to-surface mapping is then recovered that matches surfaces in 3D. Lastly, we use a spectral method that ensures that the grids induced on the target surface remain conformal, i.e., using the chain rule, we express the gradient of the mutual information between surfaces in the conformal basis of the source surface so that the updated parameterization remains conformal.

4. Multivariate Tensor-based Morphometry

4.1. Derivative Map

Suppose $\phi : S_1 \rightarrow S_2$ is a map from the surface S_1 to the surface S_2. To simplify the formulation, we use the isothermal coordinates of both surfaces for the arguments. Let $(u_1, v_1), (u_2, v_2)$ be the isothermal coordinates of S_1 and S_2 respectively. The Riemannian metric of S_i is represented as $\mathbf{g}_i = e^{2\lambda_i}(du_i^2 + dv_i^2), i = 1, 2$.

In the local parameters, the map ϕ can be represented as $\phi(u_1, v_1) = (\phi_1(u_1, v_1), \phi_2(u_1, v_1))$. The *derivative map* of ϕ is the linear map between the tangent spaces, $d\phi : TM(p) \rightarrow TM(\phi(p))$, induced by the map ϕ. In the local parameter domain, the derivative map is the Jacobian of ϕ,

$$d\phi = \begin{pmatrix} \frac{\partial \phi_1}{\partial u_1} & \frac{\partial \phi_1}{\partial v_1} \\ \frac{\partial \phi_2}{\partial u_1} & \frac{\partial \phi_2}{\partial v_1} \end{pmatrix}.$$

Let the position vector of S_1 be $\mathbf{r}(u_1, v_1)$. Denote the tangent vector fields as $\frac{\partial}{\partial u_1} = \frac{\partial \mathbf{r}}{\partial u_1}, \frac{\partial}{\partial v_1} = \frac{\partial \mathbf{r}}{\partial v_1}$. Because (u_1, v_1) are isothermal coordinates, $\frac{\partial}{\partial u_1}$ and $\frac{\partial}{\partial v_1}$ only differ by a rotation of $\pi/2$. Therefore, we can construct an orthonormal frame on the tangent plane on S_1 as $\{e^{-\lambda_1}\frac{\partial}{\partial u_1}, e^{-\lambda_1}\frac{\partial}{\partial v_1}\}$. Similarly, we can construct an orthonormal frame on S_2 as $\{e^{-\lambda_2}\frac{\partial}{\partial u_2}, e^{-\lambda_2}\frac{\partial}{\partial v_2}\}$.

The derivative map under the two orthonormal frames (for S_1 and S_2) can be written as

$$d\phi = e^{\lambda_2 - \lambda_1} \begin{pmatrix} \frac{\partial \phi_1}{\partial u_1} & \frac{\partial \phi_1}{\partial v_1} \\ \frac{\partial \phi_2}{\partial u_1} & \frac{\partial \phi_2}{\partial v_1} \end{pmatrix}.$$

In practice, smooth surfaces are usually approximated by triangle meshes. The map ϕ is approximated by a simplicial map, which maps vertices to vertices, edges to edges and faces to faces. The derivative map $d\phi$ is approximated by the linear map from one face $[v_1, v_2, v_3]$ to another one $[w_1, w_2, w_3]$. First, we isometrically embed the triangle $[v_1, v_2, v_3]$,$[w_1, w_2, w_3]$ onto the plane $\mathbb{R}^2$; the planar coordinates of the vertices of v_i, w_j are denoted using the same symbols v_i, w_j. Then we explicitly compute the linear matrix for the derivative map $d\phi$,

$$d\phi = [w_3 - w_1, w_2 - w_1][v_3 - v_1, v_2 - v_1]^{-1}. \quad (2)$$

4.2. Multivariate Tensor-Based Statistics

In our work, we use multivariate statistics on deformation tensors [12] and adapt the concept to surface tensors. Let J be the derivative map and define the deformation tensors as $S = (J^T J)^{1/2}$. Instead of analyzing shape change based on the eigenvalues of the deformation tensor, we consider a new family of metrics, the "Log-Euclidean metrics" [1]. These metrics make computations on tensors easier to perform, as they are chosen such that the transformed values form a vector space, and statistical parameters can then be computed easily using standard formulae for Euclidean spaces.

We apply Hotelling's T^2 test on sets of values in the log-Euclidean space of the deformation tensors. Given two groups of n-dimensional vectors S_i, $i = 1, ..., p$, T_j, $j = 1, ..., q$, we use the Mahalanobis distance M to measure the group mean difference,

$$M = (log\bar{S} - log\bar{T})\Sigma^{-1}(log\bar{S} - log\bar{T}) \quad (3)$$

where $\bar{S}$ and $\bar{T}$ are the means of the two groups and Σ is the combined covariance matrix of the two groups.

5. Experimental Results

We applied the multivariate TBM method to various anatomical surfaces extracted from 3D MRI scans of the brain. For registering anatomical surfaces across subjects, holomorphic one-form based segmentation method works better for parameterizing long, cylinder-like shapes, such as hippocampal and lateral ventricular surfaces. In the light of this observation, we used a holomorphic one-form to conformally map hippocampal and lateral ventricular surfaces to a set of planar rectangles (subsection 5.1 and 5.2). Through the parameter domain, we can register surfaces by using a constrained harmonic mapping and a surface fluid registration method. Figure 2 illustrates the surface conformal parameterizations for two different brain anatomical structures (algorithm details can be found at [22]). In Figure 2 (a), we compare two conformal parameterization results on a left hippocampal surface, the left shows results from the canonical holomorphic one-form and the right

	Full Matrix J	Determinant of J	Largest EV of J	Pair of EV of J
Left Hippo Surface	**0.0069**	0.1495	0.0429	0.0376
Right Hippo Surface	**0.0303**	0.0873	0.1164	0.0715
Left Vent Surface	**0.0028**	0.0330	0.0098	0.0084
Right Vent Surface	**0.0066**	0.0448	0.0120	0.0226

Table 1. Permutation-based overall significance p value for two experiments (J is the Jacobian matrix and EV stands for Eigenvalue. To detect group differences, it was advantageous to use the full tensor, or its two eigenvalues together; with simpler local measures based on surface area, group differences were missed.).

shows from spherical conformal mapping [9]. Both parameterizations are visualized by the texture mapping of the checker board. The holomorphic one-form parameterization result is more uniform than the spherical one. It helps generate more accurate surface mapping results. Figure 2 (b) illustrates how we use the canonical holomorphic one-form to register a left lateral ventricular surface. (c) illustrates a comparison of the surface segmentation results on a pair of lateral ventricular surfaces from two different groups, an HIV/AIDS individual (up) and a matched control subject (bottom). In the figure, each segment is labeled by a unique color and surfaces are registered by matching each component segment. The ventricular surfaces are dilated due to the disease. Since their overall surface structures are still similar, our holomorphic differential based algorithm successfully registered them consistently.

In this paper, the segmentations are regarded as given, and results are from automated and manual segmentations detailed in other prior works [18, 17].

5.1. Multivariate Tensor-Based Morphometry on Hippocampal Surfaces: Application to Alzheimer's Disease

The hippocampal surface is a structure in the medial temporal lobe of the brain. Parametric shape models of the hippocampus are commonly developed for tracking shape differences or longitudinal atrophy in disease. Many prior studies, e.g., [18, 13], have shown that there is atrophy as the disease progresses. In our method, we leave two holes on the front and back of the hippocampal surface, representing its anterior junction with the amygdala, and its posterior limit as it turns into the white matter of the fornix. It can then be logically represented as an open boundary genus-one surface, i.e., a cylinder. Its canonical holomorphic one-form can be easily computed. By integrating this holomorphic one-form, it can be conformally mapped to a rectangle. By considering intrinsic geometric feature alignment, a surface fluid registration method [23] achieved better registration results than our prior work [20].

Figure 3 illustrates our experimental results on a group of hippocampal surface models extracted from 3D brain MRI scans of 12 AD individuals and 14 control subjects [18]. After surface registration, we ran a permutation test with

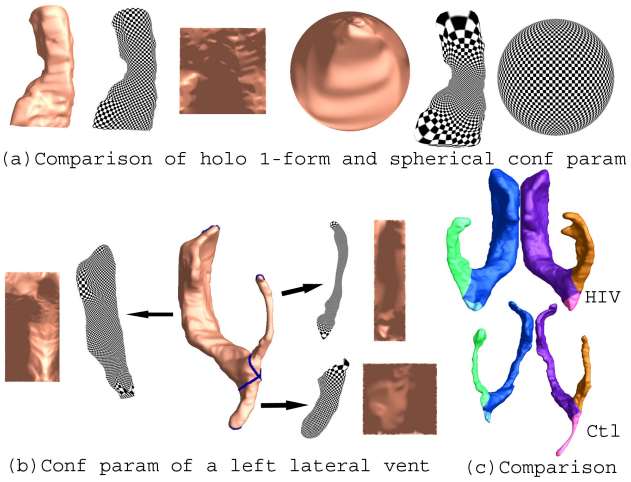

Figure 2. The first row illustrates how a holomorphic 1-form conformally maps a left hippocampal surface to a rectangle. The second row illustrates how a holomorphic 1-form conformally splits a left lateral ventricular surface to three component parts, and maps each of them conformally to a rectangle. The third row illustrates the computed exact harmonic 1-form (a), conjugate harmonic 1-form (b) and holomorphic 1-form that conformally maps a cortical surface to a slit map.

$5,000$ random assignments of subjects to groups to estimate the statistical significance of the areas with group differences in surface morphometry. We also used a statistical threshold of $p = 0.05$ at each surface point to compute the supra-threshold surface area, and we estimate the overall significance of the experimental results by using a non-parametric permutation test to establish an empirical null distribution for this surface area [19]. Although the samples sizes are small, we still detected relatively large statistically significant areas, consistent with prior findings [18]. The overall statistical significance p-values, based on permutation testing (and therefore corrected for multiple comparisons), were 0.0069 for the left hippocampal surface and 0.0303 for the right hippocampal surface (Figure 3 (a)).

5.2. Multivariate Tensor-Based Morphometry of the Ventricular Surface in HIV/AIDS

The lateral ventricles are often enlarged in disease and can provide sensitive measures of disease progression [17,

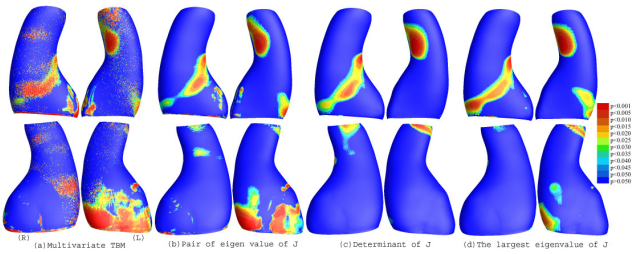

Figure 3. Comparison of various tensor-based morphometry results on a group of hippocampal surfaces from 12 AD patients and 14 matched control subjects. Each panel is associated with a different TBM metric. Each row is the same surface viewed from the bottom and the top, respectively. In all cases, multivariate statistics on the full metric tensor detected anatomical differences more powerfully than simple univariate surface measures. Overall statistical significance values (corrected for multiple comparisons) are listed in Table 1.

3]. Ventricular changes reflect atrophy in surrounding structures, so ventricular measures and surface-based maps provide sensitive assessments of tissue reduction that correlate with cognitive deterioration in illnesses. However, the concave shape, complex branching topology and extreme narrowness of the inferior and posterior horns have made it difficult for surface parametrization approaches to impose a grid on the entire structure without introducing significant area distortion. To model the lateral ventricular surface, we automatically locate and introduce three cuts on each ventricle. The cuts are motivated by examining the topology of the lateral ventricles, in which several horns are joined together at the ventricular "atrium" or "trigone". We call this topological modeling step, interpreting the ventricles as a set of connected, simpler surfaces, a *topology optimization* operation. The topological optimization helps to enable a uniform parametrization in some areas that otherwise are very difficult to capture with usual parametrization methods. After the topology is modeled in this way, a lateral ventricular surface, in each hemisphere, becomes an open boundary surface with 3 boundaries. We computed the canonical holomorphic one-form (Eqn. 1). With holomorphic flow segmentation [22], each lateral ventricular surface can be divided into 3 pieces. Although surface geometry is widely variable across subjects, the zero point locations are intrinsically determined by the surface conformal structures, and the partitioning of the surface into component meshes is highly consistent across subjects. After the surface segmentation, each lateral ventricular surface is divided to three surfaces, each topologically equivalent to a cylinder. For each piece, we again applied the holomorphic flow algorithm to it and conformally mapped it to a rectangle and register them with a constrained harmonic map.

In our experiments, we compared ventricular surface models extracted from 3D brain MRI scans of 11 HIV/AIDS individuals and 8 control subjects [17]. After surface registration, we computed the surface Jacobian matrix and applied multivariate tensor-based statistics to study differences in ventricular surface morphometry. We ran a permutation test with $5,000$ random assignments of subjects to groups to estimate the statistical significance of the areas with group differences in surface morphometry. We also used a statistical threshold of $p = 0.05$ at each surface point to estimate the overall significance of the experimental results by non-parametric permutation test [19]. The experimental results are shown in Figure 4(a). Although sample sizes are small, we still detected large statistically significant areas, consistent with prior findings [17]. The overall statistical significance p-values, based on permutation testing, were 0.0022 for the left lateral ventricle and 0.008 for the right lateral ventricle [20].

5.3. Biomarker Detection for HIV/AIDS Ventricular Surface Morphometry

Biomarkers are a set of biology features that can help screening and early diagnosis of diseases. Ferrarini et al. [8] studied biomarkers for lateral ventricular surface for AD. Based on our multivariate TBM results, we picked up a set of vertex that are statistically significant in the obtained p-map. We used this set of vertex as biomarkers to classify a new surface based on its multivariate TBM statistics. In our experiments, first, we sorted all vertex according their p values from low to high. We select a certain number of vertices (e.g. 1% of overall vertices) with the smallest p values as the biomarkers. With a distance calculated by Equation 3, we ran leave-on-out tests with the Nearest Neighbor classifier on left and right ventricular surfaces. For 1% of the whole vertex set, about 271 vertices as biomarkers, we successfully classified all 11 HIV patient surfaces on both sides. Overall, we achieved a 100% sensitivity on both right and left lateral ventricular surfaces; and 100% and 87.5% specificity on right and left, respectively.

5.4. Comparison with Other TBM methods

To explore whether our multivariate statistics provided extra power when running TBM on the surface data, in each experiment, we also conducted three additional statistical tests based on different tensor-based statistics derived from the Jacobian matrix. The other statistics we studied were: (1) the determinant of Jacobian matrix; (2) the largest eigenvalue of Jacobian matrix; and (3) the pair of eigenvalues of the Jacobian matrix, treated as a 2-component vector. For statistics (1) and (2), we applied a Students t test to compute the group mean difference at each surface point. In case (3), we used Hotelling's T^2 statistics to compute the group mean difference. For the three new statistics, their calculated statistical maps are shown in Figure 3, 4, respectively. For each statistic, we also computed the overall p-values

(see Table 1). In each experiment, the overall localization and spatial pattern of surface abnormalities detected by different tensor-based surface statistics were highly consistent.

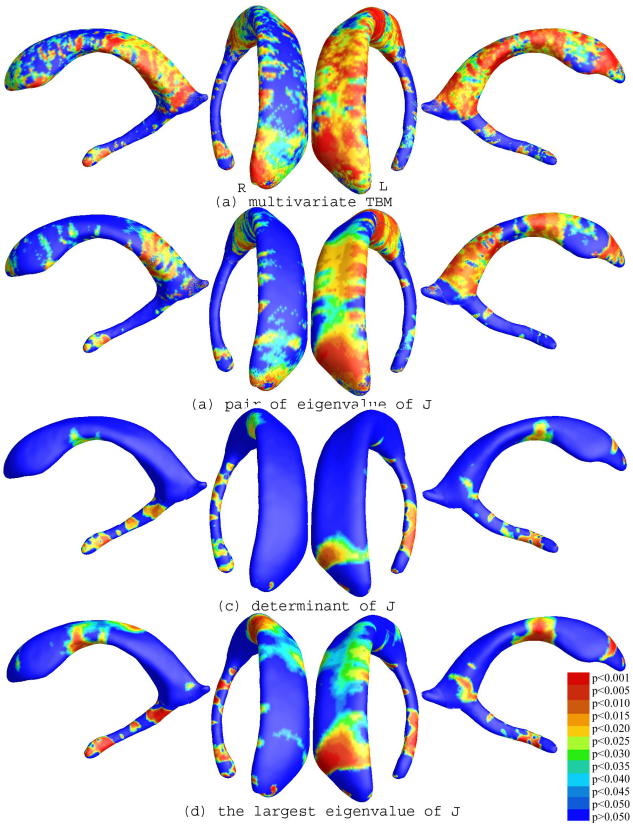

Figure 4. Comparison of various tensor-based morphometry results on a group of lateral ventricular surfaces from 11 HIV/AIDS patients and 8 matched control subjects. Multivariate statistics on the full metric tensor detected anatomical differences more powerfully than standard scalar statistics. Overall statistical significance values (corrected for multiple comparisons) are listed in Table 1.

We also conducted biomarker experiments based on the p-map results from three tensor-based statistical tests. Each time, we selected the same number of vertex that are most statistically significant different between two groups as the biomarkers. We calculated L^2 norm as the distance metric and did a leave-one-out test with the Nearest Neighbor classifier on each lateral ventricular surface. Figure 5 illustrates various sensitivity rates, i.e., the rate that a surface from HIV/AIDS group was successfully classified, with different number of biomarkers for four statistics. The results show that the full tensor metric based biomarkers achieved a 100% sensitivity and outperformed results of all three statistics. The results on the specificity are similar and ignored here due to the space limitation.

In summary, both experiments strongly suggested that the newly proposed multivariate TBM method has more detection power in terms of effect size (and the area with suprathreshold statistics), probably because it captures more directional and rotational information when measuring geometric differences.

6. Conclusion and Future Work

In this paper, we presented a multivariate tensor-based morphometry framework for analyzing parametric surfaces. Holomorphic differentials there were computed with better numerical accuracy were used to register anatomical structures. We applied this framework to detect surface regions with abnormal brain structure in groups of AD and HIV/AIDS individuals versus matched healthy controls. The empirical results suggest that our method may outperform TBM methods based on simpler univariate surface measures. In future, we will apply this multivariate TBM framework to additional 3D MRI datasets to study brain surface morphometry and general shape analysis.

Acknowledgement: This work was funded by National Institute of Health through the NIH Roadmap for Medical Research, Grant U54 RR021813 entitled Center for Computational Biology (CCB).

References

[1] V. Arsigny, P. Fillard, X. Pennec, and N. Ayache. Log-Euclidean metrics for fast and simple calculus on diffusion tensors. In *Magn. Reson. Med.*, volume 56, pages 411–421, 2006.

[2] J. Ashburner, C. Hutton, R. Frackowiak, I. Johnsrude, C. Price, and K. Friston. Identifying global anatomical differences: deformation-based morphometry. *Human Brain Mapping*, 6(5-6):348–357, 1998.

[3] Y. Chou, N. Leporé, G. I. de Zubicaray, O. T. Carmichael, J. T. Becker, A. W. Toga, and P. M. Thompson. Automated ventricular mapping with multi-atlas fluid image alignment reveals genetic effects in Alzheimer's disease. *NeuroImage*, 40(2):615 – 630, 2008.

[4] M. Chung, K. Dalton, and R. Davidson. Tensor-based cortical surface morphometry via weighted spherical harmonic representation. *IEEE Trans. Med. Imag.*, 27(8):1143–1151, Aug. 2008.

[5] M. K. Chung, K. J. Worsley, S. Robbins, T. Paus, J. Taylor, J. N. Giedd, J. L. Rapoport, and A. C. Evans. Deformation-based surface morphometry applied to gray matter deformation. *NeuroImage*, 18(2):198 – 213, 2003.

[6] A. M. Dale, B. Fischl, and M. I. Sereno. Cortical surface-based analysis I: segmentation and surface reconstruction. *Neuroimage*, 9:179–194, 1999.

[7] C. Davatzikos, M. Vaillant, S. M. Resnick, J. L. Prince, S. Letovsky, and R. N. Bryan. A computerized approach for morphological analysis of the corpus callosum. *J Comput Assist Tomogr*, 20(1):88–97, 1996.

[8] L. Ferrarini, W. M. Palm, H. Olofsen, R. van der Landen, M. A. van Buchem, J. H. Reiber, and F. Admiraal-

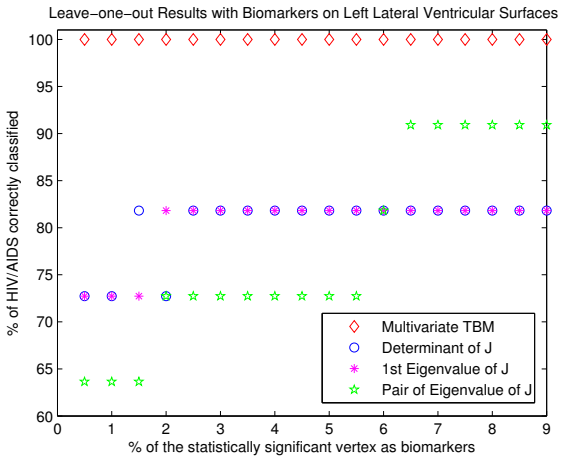

(a)

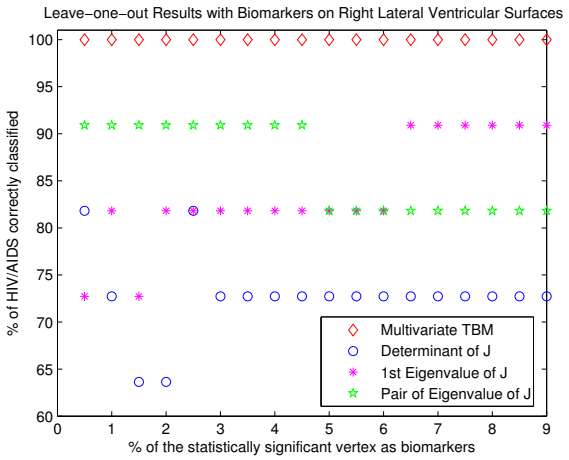

(b)

Figure 5. Comparison of leave-one-out HIV/AIDS classification results using detected biomarkers from various tensor-based morphometry results on a group of lateral ventricular surfaces from 11 HIV/AIDS patients and 8 matched control subjects. (a) and (b) are the results on left and right ventricles, respectively. Biomarkers from full metric tensor are more powerful to detect surfaces from the HIV/AIDS group.

Behloul. Ventricular shape biomarkers for Alzheimer's disease in clinical MR images. *Magnetic resonance in medicine*, 59(2):260–7, 2008.

[9] X. Gu, Y. Wang, T. F. Chan, P. M. Thompson, and S.-T. Yau. Genus zero surface conformal mapping and its application to brain surface mapping. *IEEE Trans. Med. Imag.*, 23(8):949–958, Aug. 2004.

[10] M. Holden. A review of geometric transformations for nonrigid body registration. *IEEE Trans. Med. Imag.*, 27(1):111–128, Jan. 2008.

[11] I. Kakadiaris, G. Passalis, G. Toderici, M. Murtuza, Y. Lu, N. Karampatziakis, and T. Theoharis. Three-dimensional face recognition in the presence of facial expressions: An annotated deformable model approach. *IEEE Trans. Pattern Anal. and Machine Intell.*, 29(4):640–649, April 2007.

[12] N. Leporé, C. Brun, Y.-Y. Chou, M.-C. Chiang, R. A. Dutton, K. M. Hayashi, E. Luders, O. L. Lopez, H. J. Aizenstein, A. W. Toga, J. T. Becker, and P. M. Thompson. Generalized tensor-based morphometry of HIV/AIDS using multivariate statistics on deformation tensors. *IEEE Trans. Med. Imag.*, 27(1):129–141, Jan. 2008.

[13] J. Morra, Z. Tu, L. Apostolova, A. Green, C. Avedissian, S. Madsen, N. Parikshak, A. Toga, C. Jack, N. Schuff, M. Weiner, and P. Thompson. Automated mapping of hippocampal atrophy in 1-year repeat MRI data in 490 subjects with Alzheimer's disease, mild cognitive impairment, and elderly controls. *NeuroImage*, Nov. 8 2008.

[14] U. Pinkall and K. Polthier. Computing discrete minimal surfaces and their conjugate. In *Experimental Mathematics 2 (1)*, pages 15–36, 1993.

[15] K. Strebel. *Quadratic Differentials*. Springer, 1984.

[16] P. Thompson and A. Toga. A surface-based technique for warping 3-dimensional images of the brain. *IEEE Trans. Med. Imag.*, 15(4):1–16, 1996.

[17] P. M. Thompson, R. A. Dutton, K. M. Hayashi, A. Lu, S. E. Lee, J. Y. Lee, O. L. Lopez, H. J. Aizenstein, A. W. Toga, and J. T. Becker. 3D mapping of ventricular and corpus callosum abnormalities in HIV/AIDS. *NeuroImage*, 31(1):12–23, 2006.

[18] P. M. Thompson, K. M. Hayashi, G. I. de Zubicaray, A. L. Janke, S. E. Rose, J. Semple, M. S. Hong, D. H. Herman, D. Gravano, D. M. Doddrell, and A. W. Toga. Mapping hippocampal and ventricular change in Alzheimer's disease. *NeuroImage*, 22(4):1754 – 1766, 2004.

[19] P. M. Thompson, A. D. Lee, R. A. Dutton, J. A. Geaga, K. M. Hayashi, M. A. Eckert, U. Bellugi, A. M. Galaburda, J. R. Korenberg, D. L. Mills, A. W. Toga, and A. L. Reiss. Abnormal cortical complexity and thickness profiles mapped in Williams syndrome. *J. Neuroscience*, 25(16):4146–4158, 2005.

[20] Y. Wang, T. F. Chan, A. W. Toga, and P. M. Thompson. Multivariate tensor-based brain anatomical surface morphometry via holomorphic one-forms. *Med. Image Comp. Comput.-Assist. Intervention, Proceedings*, 2009.

[21] Y. Wang, X. Gu, T. F. Chan, P. M. Thompson, and S.-T. Yau. Conformal slit mapping and its applications to brain surface parameterization. *Med. Image Comp. Comput.-Assist. Intervention, Proceedings, Part I*, pages 585–593, 2008. LNCS 5241.

[22] Y. Wang, L. M. Lui, X. Gu, K. M. Hayashi, T. F. Chan, A. W. Toga, P. M. Thompson, and S.-T. Yau. Brain surface conformal parameterization using Riemann surface structure. *IEEE Trans. Med. Imag.*, 26(6):853–865, June 2007.

[23] Y. Wang, Y. Wang, M. Chiang, T. F. Chan, A. W. Toga, and P. M. Thompson. Surface fluid registration for brain mapping research. Under Preparation.

[24] W. Zeng, Y. Zeng, Y. Wang, X. Yin, X. Gu, and D. Samaras. 3D non-rigid surface matching and registration based on holomorphic differentials. In *ECCV '08: Proceedings of the 10th European Conference on Computer Vision*, pages 1–14, 2008.